RESEARCH PAPER

Channels 8:1, 35–48; January/February 2014; © 2014 Landes Bioscience

The calcium release-activated calcium channel Orai1 represents a crucial component in hypertrophic compensation and the development of dilated cardiomyopathy

Jaime S Horton[1,2], Cadie L Buckley[1,3], Ernest M Alvarez[1,2], Anita Schorlemmer[1,3], and Alexander J Stokes[1,2,3,4,*]

[1]Laboratory of Experimental Medicine; John A. Burns School of Medicine; University of Hawaii; Honolulu, HI USA; [2]Department of Cell & Molecular Biology; John A. Burns School of Medicine; University of Hawaii; Honolulu, HI USA; [3]Department of Molecular Biosciences & Bioengineering; University of Hawaii; Honolulu, HI USA; [4]Chaminade University; Honolulu, HI USA

Keywords: CRACM1, Orai1, ICRAC, pressure overload, dilated cardiomyopathy, contraction coupling, apoptosis

As exceptionally calcium selective store-operated channels, Orai channels play a prominent role in cellular calcium signaling. While most studied in the immune system, we are beginning to recognize that Orai1 provides unique calcium signaling pathways in numerous tissue contexts. To assess the involvement of Orai1 in cardiac hypertrophy we used transverse aortic constriction to model pressure overload cardiac hypertrophy and heart failure in Orai1 deficient mice. We demonstrate that Orai1 deficient mice have significantly decreased survival in this pressure overload model. Transthoracic echocardiography reveals that Orai1 deficient mice develop rapid dilated cardiomyopathy, with greater loss of function, and histological and molecular data indicate that this pathology is associated with significant apoptosis, but not major differences in cellular hypertrophy, fibrosis, and some major hypertrophic makers. Orai1 represents a crucial calcium entry mechanism in the compensation of the heart to pressure overload over-load, and the development of dilated cardiomyopathy.

Introduction

Orai1 is an excellent candidate for mediating critical calcium responses

Orai homologs, especially Orai1, represent major routes for entry of extracellular Ca^{2+} entry across the plasma membrane. The Orai calcium channel is composed of a hexameric assembly of Orai subunits around a central ion pore, which crosses the membrane and extends into the cytosol, with extracellular glutamate residues forming a selectivity filter.[1] Orai channels contain 4 transmembrane spanning regions, and this and the hexameric arrangement of Orai subunits contrasts distinctly from many other ion channels, such as the 6 membrane-spanning helices and tetrameric subunit character of the TRP (transient receptor potential) channels, which were initially expected to comprise the channel protein responsible for the I_{CRAC} current (Calcium-Release Activated Calcium Current).[2] Inositol 1,4,5-trisphosphate (Ins(1,4,5)P_3)-mediated depletion of Ca^{2+} from the endoplasmic reticulum (ER) stores results in oligomerization of the recently defined stromal interacting molecule 1 (STIM1), the ER Ca^{2+} sensor directly coupled to Orai1. Direct Stim1 - Orai1 interaction activates Orai1, and subsequently the I_{CRAC} current (Calcium-Release Activated Calcium Current) develops, leading directly to a sustained increase of intracellular Ca^{2+} concentrations and long-term functional consequences.[2-9] As I_{CRAC} was initially described in mast cells and lymphocytes,[8,9] long before its molecular identity was discovered,[2] studies in cells of the immune system are abundant, including T cells, NK cells, B cells, and mast cells, where the I_{CRAC} Ca^{2+} signals control activation, differentiation, proliferation, apoptosis and a variety of transcriptional programs.[6,7,10-13]

Cellular distribution of Orai1 in the heart: Multiple candidate populations in which Orai1 could impact the heart physiology

Orai1 is known to play a role in 2 of the major cell types that can affect outcomes in heart failure pathology; myocytes and leukocytes such as T cells, macrophages, and mast cells. Muscle cells such as vascular smooth muscle cells and especially cardiomyocytes are obviously key players in the major structural changes of the heart and circulatory system that accompany multiple cardiac pathologies. Notably, cardiac hypertrophy is classically considered to be an adaptive and compensatory response that increases the work output of cardiomyocytes and thus maintains cardiac function despite increased load.

*Correspondence to: Alexander James Stokes; Email: astokes@hawaii.edu
Submitted: 08/15/2013; Revised: 09/13/2013; Accepted: 09/23/201; Published Online: 10/17/2013
http://dx.doi.org/10.4161/chan.26581

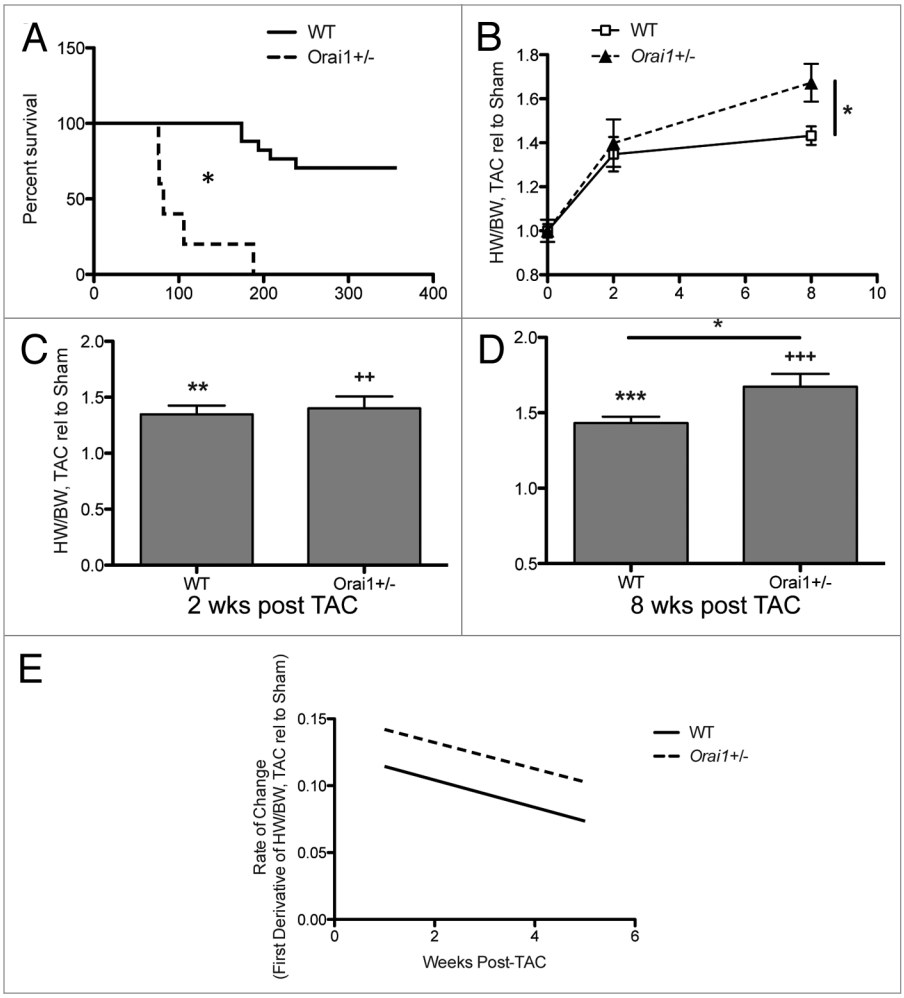

Figure 1. Survival and gravimetric analysis of hearts from TAC and sham treated *Orai1*$^{+/-}$ and WT mice. (**A**) Survival analysis of TAC treated WT, and *Orai1*$^{+/-}$ mice. Kaplan–Meier survival curves presenting the percentage of mice surviving at each time point post TAC treatment for WT vs. *Orai1*$^{+/-}$ mice ($p = < 0.0001$, $n = 5,8$). (**B**) Heart weight/body weight (HW/BW) in TAC treated relative to sham treated *Orai1*$^{+/-}$ and WT mice from 0 to 8 weeks post TAC ($p = 0.0136$). Heart weight/body weight (HW/BW) in TAC treated relative to sham treated *Orai1*$^{+/-}$ and WT mice (**C**) 2 weeks post TAC (**$p = 0.0013$, $^{**}p = 0.0039$), and (**D**) 8 weeks post TAC (***$p < 0.0001$, $^{+++}p < 0.0001$; *$p = 0.0136$). (**E**) Rate of change in HW/BW, TAC relative to sham.

Leukocytes, on the other hand, act as key components of the repair and inflammatory responses that contribute to the pathological remodeling that occurs in cardiac hypertrophy and heart failure, while assisting in beneficial and appropriate tissue repair and remodeling in myocardial infarction and injury. For example, mast cell knockout mice (cKit$^{-/-;}$ WBB6F1/J-*Kit*^{W}/*Kit*$^{W\text{-}v14}$) are provided protection from hypertrophy, but show susceptibility to infarction.[14-16]

Orai1 effects in the development of hypertrophy: conflicting in vitro and in vivo data

In cardiac, as well as skeletal muscle, store operated calcium influx through Orai1 is thought to allow the myocyte to activate calcium signaling pathways in order to respond to the changing demands of the mycocyte. Specifically this provides the essential reservoir of calcium needed for the signaling and activation of Ca^{2+}-dependent gene expression in muscle development, hypertrophy and remodeling.[17] Orai1 in cardiomyocytes is well placed to receive regulation in hypertrophic situations via stretch activated PKC, as Orai1 is a known target of PKC phosphorylation, causing suppressed store operated calcium entry through Orai1.[18] Human mutations in Orai1 cause immunodeficiency, with myopathy characterized by hypotonia, a state of low muscle tone and reduced muscle strength.[17,19] These clinical symptoms of *Orai1* mutation seem contradictory to in vitro studies where knockdown of Orai1 is associated with protection from a hypertrophic phenotype.[20]

Recognizing the need to resolve this question, we initiated an in vivo study of the consequences of Orai1 deficiency for cardiac hypertrophy and heart failure.

Results

To evaluate a putative role for Orai1 in the progression of cardiac hypertrophy leading to heart failure, we initiated a study using a pressure overload cardiac hypertrophy model.[21] Transverse aortic constriction (TAC)[22,23] was undertaken on 8 week old male WT (C57BL/6J) controls and *Orai1*$^{+/-}$ mice. Sham control mice underwent the same procedure except for aortic constriction. Baseline pressures were assessed proximal and distal to the TAC banding site by Doppler echocardiography, to establish that banding was successful and that pressures were the same between WT and *Orai1*$^{+/-}$ mice, and were sufficient to produce hypertrophy.

Survival analysis

In comparison to WT mice, *Orai1*$^{+/-}$ mice showed significantly decreased survival after TAC treatment (**Fig. 1A**).

Gravimetric analysis of the hearts

Post-TAC heart weights were significantly heavier in *Orai1*$^{+/-}$ mice as shown by heart weights normalized to body weight, indicating a small but significant increase in heart weight at 8 weeks post TAC in *Orai1*$^{+/-}$ mice compared with WT TAC mice (**Fig. 1B**). Further, there was a significant difference between sham and TAC-treated mice, indicating that the model was sufficient to produce a response in both groups (**Fig. 1C** and **D**) and that *Orai1*$^{+/-}$ mice have a rate of change that parallels WT mice (**Fig. 1E**).

Heart structure and function

Orai1 deficient mice show a significant immediate and rapid increase in end-diastolic left ventricular internal diameter (LVIDd) compared with WT mice modeled for pressure overload

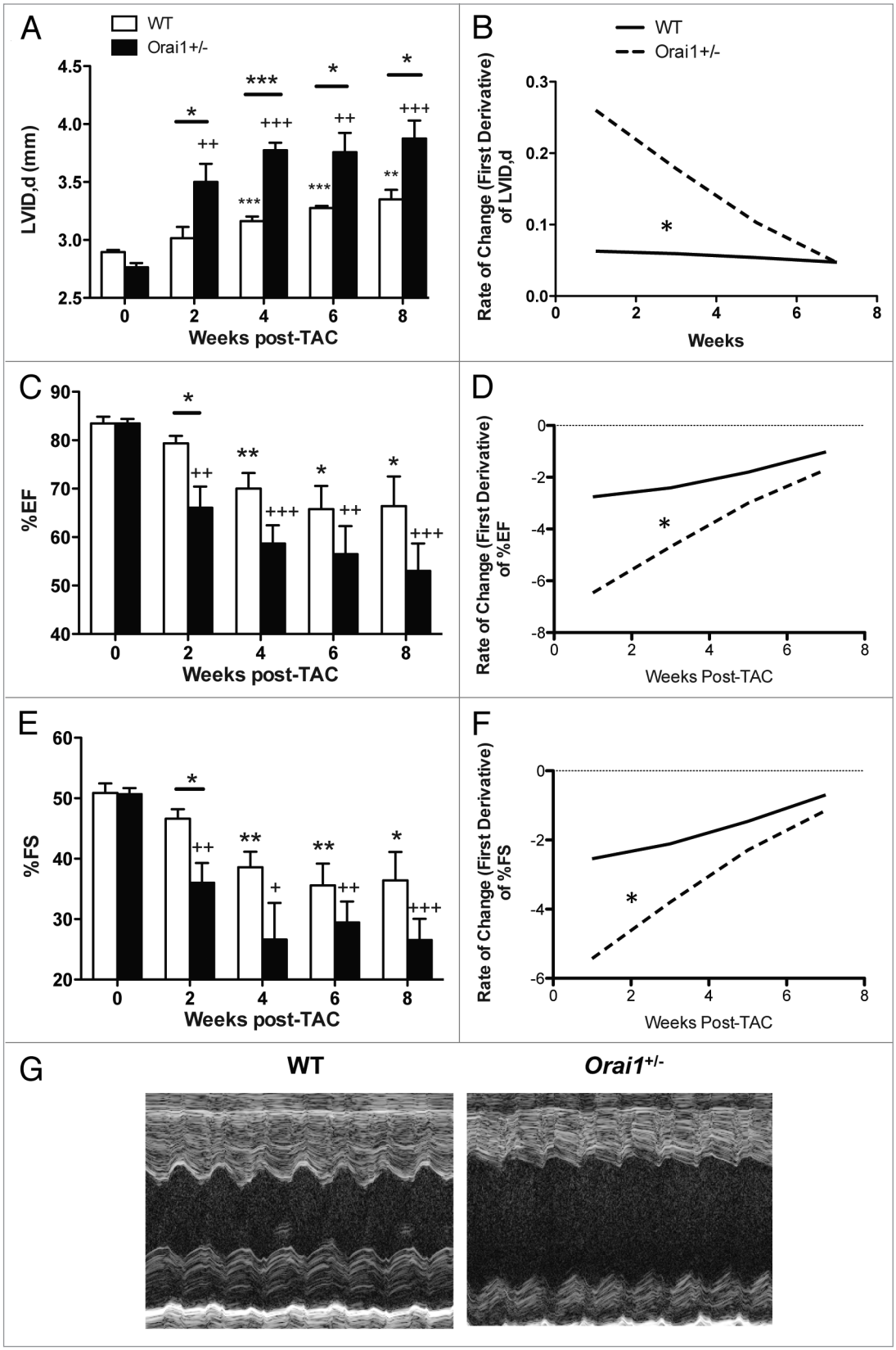

Figure 2. For figure legend, see page 38.

Figure 2 (See previous page). Heart structure and function, echocardiographic analysis of hearts from TAC and sham treated WT and *Orai1*$^{+/-}$ WT mice. (**A**) Transthoracic echocardiography analysis of left ventricular internal diameter end-diastolic (LVID,d) from 0 to 8 weeks in TAC-treated WT and *Orai1*$^{+/-}$ mice (*p = 0.0258, $^{++}$p = 0.0056, *p = 0.0434, ***p = 0.0009, $^{+++}$p < 0.0001, ***p = 0.0002, ***p < 0.0001, $^{++}$p = 0.0014, * p = 0.0384, ** p = 0.0016, $^{+++}$ p = 0.0005, * p = 0.0278, n = 4,5). (**B**) Rate of change in left ventricular internal diameter enddiastolic (LVID,d)) from 0 to 8 weeks in TAC-treated WT and *Orai1*$^{+/-}$ mice (*p < 0.001, n = 4,5). (**C**) Analysis of heart function as measured by left ventricular percent ejection fraction (%EF) ($^{++}$p = 0.0044, *p = 0.0356, **p = 0.0085, $^{+++}$p = 0.0002, *p = 0.0119, $^{++}$p = 0.0018, *p = 0.0344, $^{+++}$p = 0.0007, n = 4,5). (**D**) Rate of change in %EF (*p = 0.00066, n = 4,5) (**E**) Analysis of heart function as measured by percent fractional shortening (%FS) ($^{++}$p = 0.0077, *p = 0.0317, **p = 0.0064, $^{+}$p = 0.0116, **p = 0.0081, $^{++}$p = 0.0014, *p = 0.0266, $^{+++}$p = 0.0007) (**F**) Rate of change in %FS (*p = 0.00095, n = 4,5). (**G**) Representative echocardiography M-mode images of the left ventricle at 8 weeks in WT and *Orai1*$^{+/-}$ TAC treated mice.

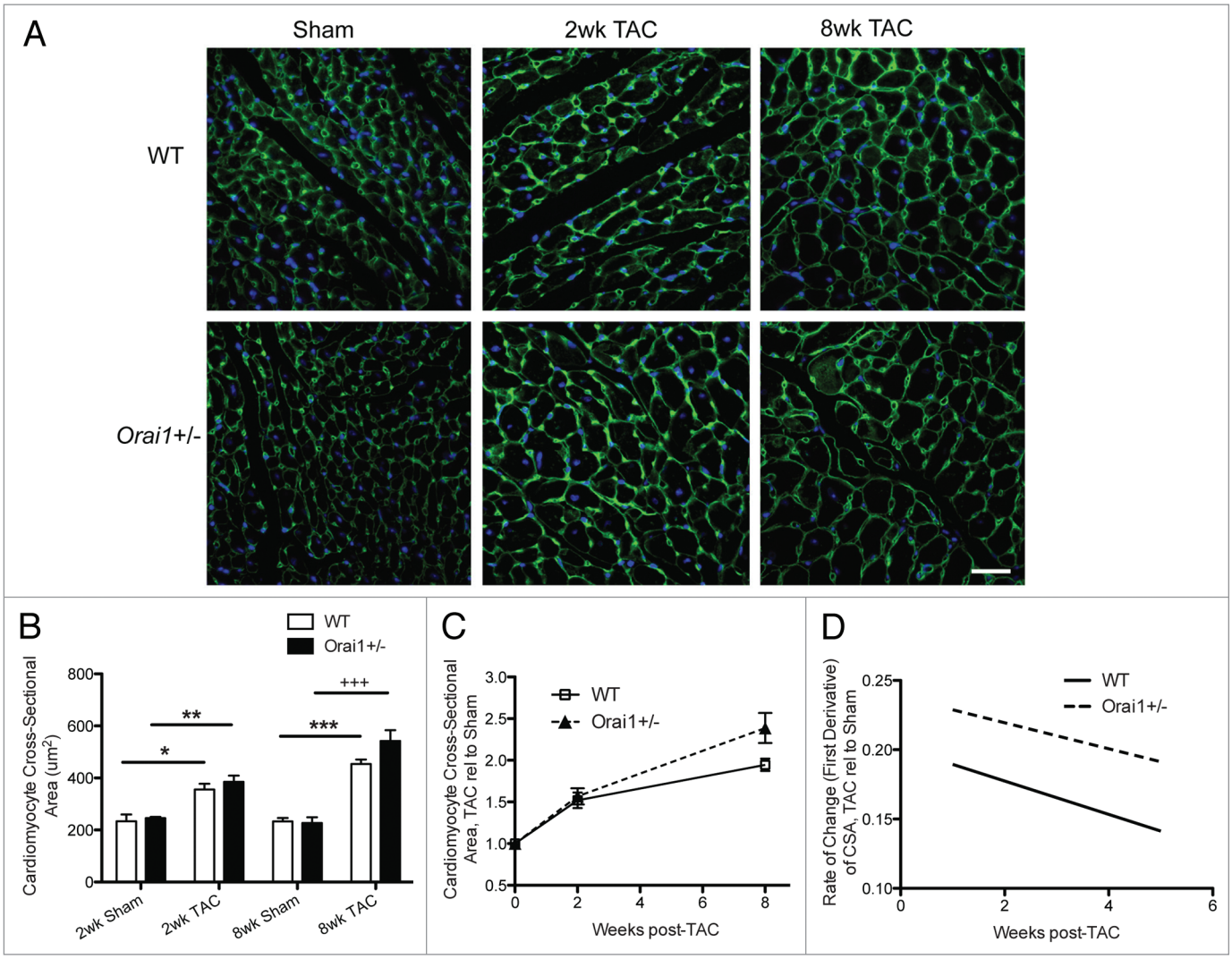

Figure 3. Cardiomyocyte cross sectional area analysis of hearts from TAC and sham treated Orai1$^{+/-}$ and WT mice. (**A**) Histological staining of sarcolemmal membrane from Sham and TAC treated WT and *Orai1*$^{+/-}$ mice. Sham WT (top left), 2 weeks TAC treated WT mice (top middle), 8 weeks TAC treated WT mice (top right), Sham *Orai1*$^{+/-}$ (bottom left), 2 weeks TAC treated *Orai1*$^{+/-}$ mice (bottom middle), and eight weeks TAC *Orai1*$^{+/-}$ mice. Green color represents plasma membrane staining (AlexaFluor-488 - wheat germ agglutinin), blue color represents the nuclei (Hoechst 33342) scale bar = 30μm. (**B**) Analysis of cardiomyocyte cross sectional area measured from histological WGA staining, from Sham and TAC treated WT and *Orai1*$^{+/-}$ mice (*p = 0.0233, **p = 0.0046, ***p = 0.0002, $^{+++}$p = 0.0005, n = 3,4). (**C**) Analysis of histological staining of cardiomyocyte cross sectional area TAC relative to Sham in WT and *Orai1*$^{+/-}$ mice (2 weeks NS, 8 weeks NS p = 0.0639, n = 3,4). (**D**) Analysis of rate of change in cardiomyocyte cross sectional area, TAC relative to Sham in WT and *Orai1*$^{+/-}$ mice.

cardiac hypertrophy and heart failure. Transthoracic echocardiographic analysis indicated a significant increase in LVIDd in *Orai1*$^{+/-}$ TAC mice vs WT TAC mice starting with a 16% greater increase at week 2 (**Fig. 2A**), with a significantly greater rate of increase in the *Orai1*$^{+/-}$ TAC mice (**Fig. 2B**). From 2 to 8 weeks post TAC, both WT TAC mice and *Orai1*$^{+/-}$ TAC mice maintained a significant increase in LVIDd compared with sham controls, and *Orai1*$^{+/-}$ TAC mice exhibited a significantly greater

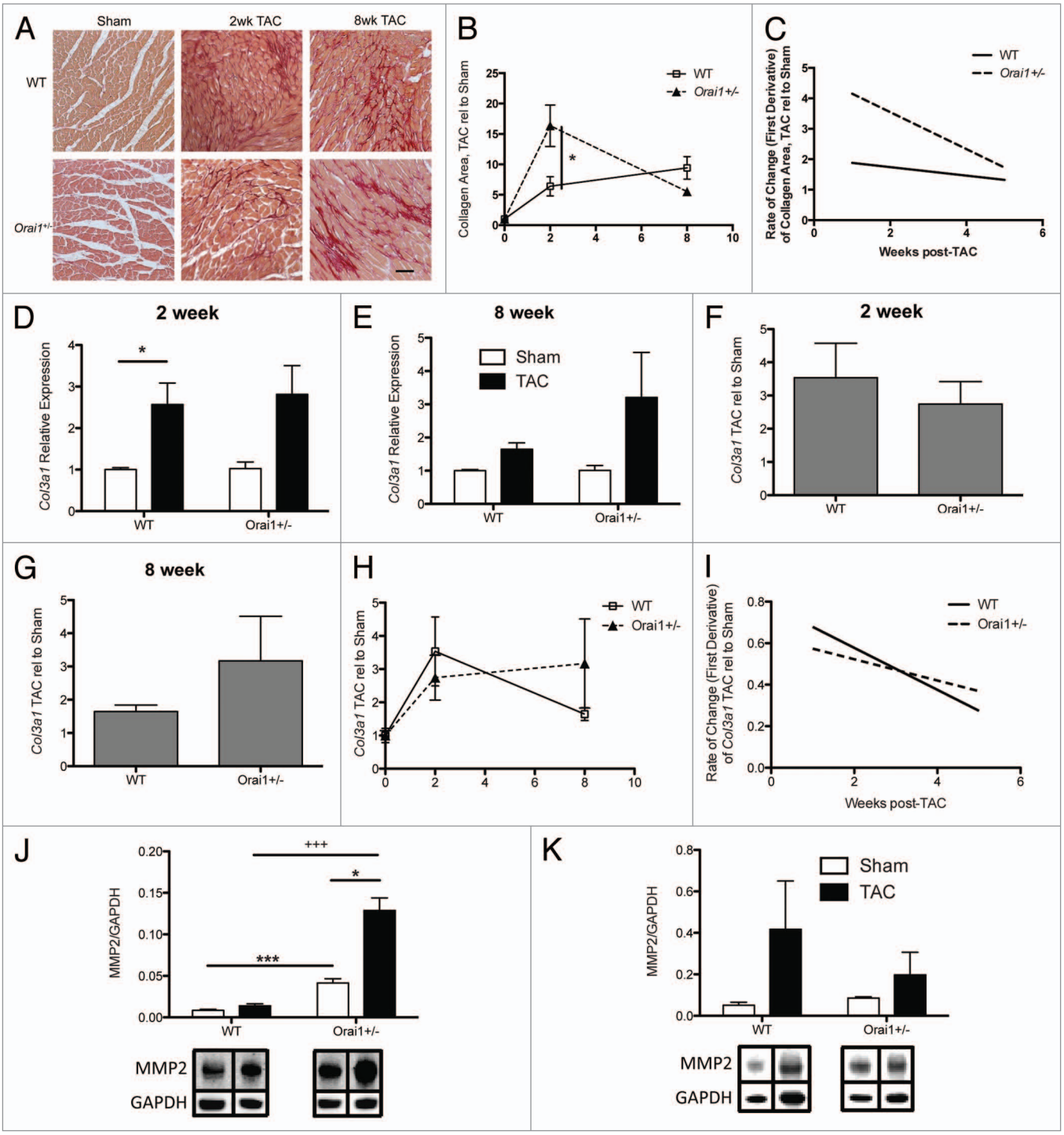

Figure 4. Expression of fibrotic and tissue remodeling markers in heart tissue lysates from TAC and sham treated *Orai1*$^{+/-}$ and WT mice. (**A**) Interstitial collagen deposition in isolated heart tissue sections stained with picrosirius red, from Sham WT (top left), 2 week TAC treated WT mice (top middle), 8 week TAC treated WT mice (top right), Sham *Orai1*$^{+/-}$ (bottom left), 2 week TAC treated *Orai1*$^{+/-}$ mice (bottom middle), and 8 week TAC *Orai1*$^{+/-}$ mice. Scale bar = 70μm. (**B**) Analysis of collagen staining by ImageJ (NIH) was used to determine the area of collagen staining as a percentage of tissue area, TAC relative to Sham (2wk NS p = 0.0569, 8wk NS p = 0.1361). (**C**) Rate of change in interstitial collagen deposition, TAC relative to Sham in WT and *Orai1*$^{+/-}$ mice. Transcriptional analysis of collagen (*Col3a1*) expression, **(D)** 2 weeks post TAC (*p = 0.039), (**E**) 8 weeks post TAC, (**F**) 2 weeks post TAC *Col3a1* expression shown as TAC relative to Sham, (NS p = 0.5475), (**G**) 8 weeks post TAC Col3a1 expression shown as TAC relative to Sham, (NS p = 0.2355). (**H**) Expression of *Col3a1* from 0 to 8 weeks, shown as TAC relative to Sham, NS (**I**) Rate of change in *Col3a1* expression, NS. Western blot densitometry analysis of matrix metalloproteinase-2 (MMP2) from TAC and sham treated *Orai1*$^{+/-}$ and WT isolated mouse heart lysates (**J**) 2 weeks post TAC (*p = 0.0222; $^{+++}$p = 0.0009; ***p = 0.0003), and **(K)** 8 weeks post TAC, (bottom panels) representative western blots with bands corresponding to MMP2 and loading control GAPDH.

increase in LVIDd compared with WT TAC mice. There was no significant change seen in sham-treated mice (data not shown).

Analysis of heart function as measured by left ventricular percent ejection fraction (%EF) and percent fractional shortening (%FS) was undertaken. The heart function of *Orai1*$^{+/-}$ TAC mice vs WT TAC mice rapidly and immediately declined by an additional 16.7% in EF, and 22.7% FS at week 2 (**Fig. 2C** and **E**), and after 2 weeks continued to decline, albeit at a slower rate (**Fig. 2D** and **F**). M-mode images of the left ventricle at 8 weeks reveal more severe dilation in *Orai1*$^{+/-}$ TAC mice than WT TAC mice (**Fig. 2G**).

Cardiomyocyte size

Despite this remarkable change in heart function, the histological analysis of heart sections shows no significant increase in cardiomyocyte cross sectional area, or rate of change in size, in isolated heart sections from *Orai1*$^{+/-}$ TAC mice as compared with WT TAC mice (**Fig. 3A, B, C, and D**). Consequently the cellular hypertrophy of cardiomyocytes in response to the increase in load is equivalent.

Fibrosis and tissue remodeling

Cardiac fibrosis and extracellular matrix (ECM) remodeling are major characteristics of pathological cardiac hypertrophy and heart failure. Excessive increases in collagens and ECM components in the interstitium and perivascular regions of the myocardium lead to a decrease in myocardial compliance and changes in electrical conduction, ultimately leading to increased risk of ventricular dysfunction and arrhythmias. Over 90% of the total collagens in the heart are the fibrillar collagens, type I and III.[24,25] Using Picosirius Red staining of heart sections from sham and TAC treated WT and *Orai1*$^{+/-}$ mice, we observe a significant increase in the amount of interstitial fibrosis in hearts from TAC-treated *Orai1*$^{+/-}$ mice compared with WT mice at 2 weeks post-TAC (**Fig. 4A** and **B**). This returns to equivalent WT levels at 8 weeks (**Fig. 4A** and **B**), and there is no significant difference in the rate of change in interstitial fibrosis (**Fig. 4C**).

Analysis of collagen (*Col3a1*) transcripts from Sham and TAC-treated WT and *Orai1*$^{+/-}$ mouse heart lysates show no significant difference in the amount of transcript at 2 and 8 weeks (**Fig. 4D** and **E**), no significant difference in TAC relative to Sham (**Fig. 4F, G,** and **H**) and no significant difference in rate of change in *Col3a1* transcripts (**Fig. 4I**) in heart lysates from Sham and TAC-treated, WT and *Orai1*$^{+/-}$ mice.

Matrix metalloproteinase (MMP)-2 synthesis is associated with, and is a direct mediator of, ventricular remodeling and failure.[26] Western blot densitometry analysis of MMP-2 indicates significantly more expression at week 2 post-TAC in heart lysates from TAC treated *Orai1*$^{+/-}$ mice than TAC treated WT mice (**Fig. 4J** and **K**). Bottom panels show representative western blots with bands corresponding to MMP2 and loading control GAPDH.

Expression of myocardial Transforming Growth Factor Beta (TGF-β) is upregulated in both experimental models of cardiac hypertrophy and in patients with dilated or hypertrophic cardiomyopathy, where it exerts pleiotropic effects on all cell types involved in cardiac insult. TGF-β enhances hypertrophic signals to cardiomyocytes, stimulates myofibroblast transdifferentiation, and enhances matrix deposition and preservation.[27] Transcriptional analysis of TGF- β transcript levels from Sham and TAC-treated, WT and *Orai1*$^{+/-}$ isolated mouse heart lysates indicate a significant upregulation in TAC *Orai1*$^{+/-}$ mice at 8 weeks post TAC (**Fig. 5D**).

Analysis of classical markers of cardiac hypertrophy and heart failure

Reactivation of the fetal gene program is a hallmark of the stressed heart, characterized by a clear upregulation of natriuretic peptides.[28,29] In the heart, atrial natriuretic peptide (ANP, *Nppa*) expression is confined to the atria, while B-type natriuretic peptide (BNP, *Nppb*) is expressed in both the atria and ventricles. C-type natriuretic peptide (CNP, *Nppc*) is produced by vascular endothelium. ANP is produced mainly by cardiomyocytes, and is a key component of cardiovascular homeostatic mechanisms such as vasodilation and natriuresis, functioning to regulate blood pressure. ANP also acts as an autocrine/paracrine factor on other tissue targets such as the kidney, lung, thymus, liver, and components of the immune system. Here in our overload model, as with patients presenting with heart failure, ANP and BNP are both elevated in tissue and plasma as the cardiac hormonal system is activated by increased wall stretch due to increased volume and pressure overload, in order to promote and regulate compensation. Transcriptional analysis of isolated heart lysates from Sham and TAC-treated *Orai1*$^{+/-}$ and WT mice indicate an earlier upregulation of *Nppa* in *Orai1*$^{+/-}$ than in WT mice (**Fig. 5A**). This is also true for western blot densitometry analysis of ANP protein levels in isolated heart lysates (**Fig. 5B**). This would indicate a greater stretch activation and attempt to respond further to the pressure overload, i.e., a need for a greater compensation response. Transcriptional regulation of *Nppb* is not significantly different in *Orai1*$^{+/-}$ compared with the WT mouse response (**Fig. 5C**).

Modeled pressure overload and clinical heart failure elicit expression of pro-inflammatory cytokines such as interleukin 1, interleukin 6 (IL-6), and tumor necrosis factor-α (TNF-α), which mediate, via specific receptors, gene expression, cell growth, and apoptosis. Chronic IL-6 stimulation leads to left ventricular hypertrophy and dysfunction, and deletion of IL-6 reduces LV hypertrophy after angiotensin II infusion. However, knockout of IL-6 alone is not sufficient to attenuate LV remodeling and dysfunction in failing hearts.[30] Similarly to ANP expression in our pressure overload model, transcriptional analysis shows that *Il-6* is also upregulated earlier in *Orai1*$^{+/-}$ than in WT mice modeled for pressure overload cardiac hypertrophy (**Fig. 5E**).

Analysis of calcium regulators

As Orai1 is 1 of 3 homologs responsible for store operated calcium influx, we initiated analysis of these and other calcium-regulating proteins, in the event that *Orai1*$^{+/-}$ mice present basal or experimental compensatory expression. Transcriptional analysis of *Stim1* (Stromal interaction molecule 1), *Serca2* (sarcoplasmic reticulum Ca^{2+}-ATPase 2), *Orai2,* and *Orai3* in isolated heart lysates from Sham WT and *Orai1*$^{+/-}$ mice indicate no significant changes in basal expression (**Fig. 6A–D**).

Stim1 functions in cells as a dynamic calcium sensor. Spanning the ER membrane, Stim1 translocates into junctions

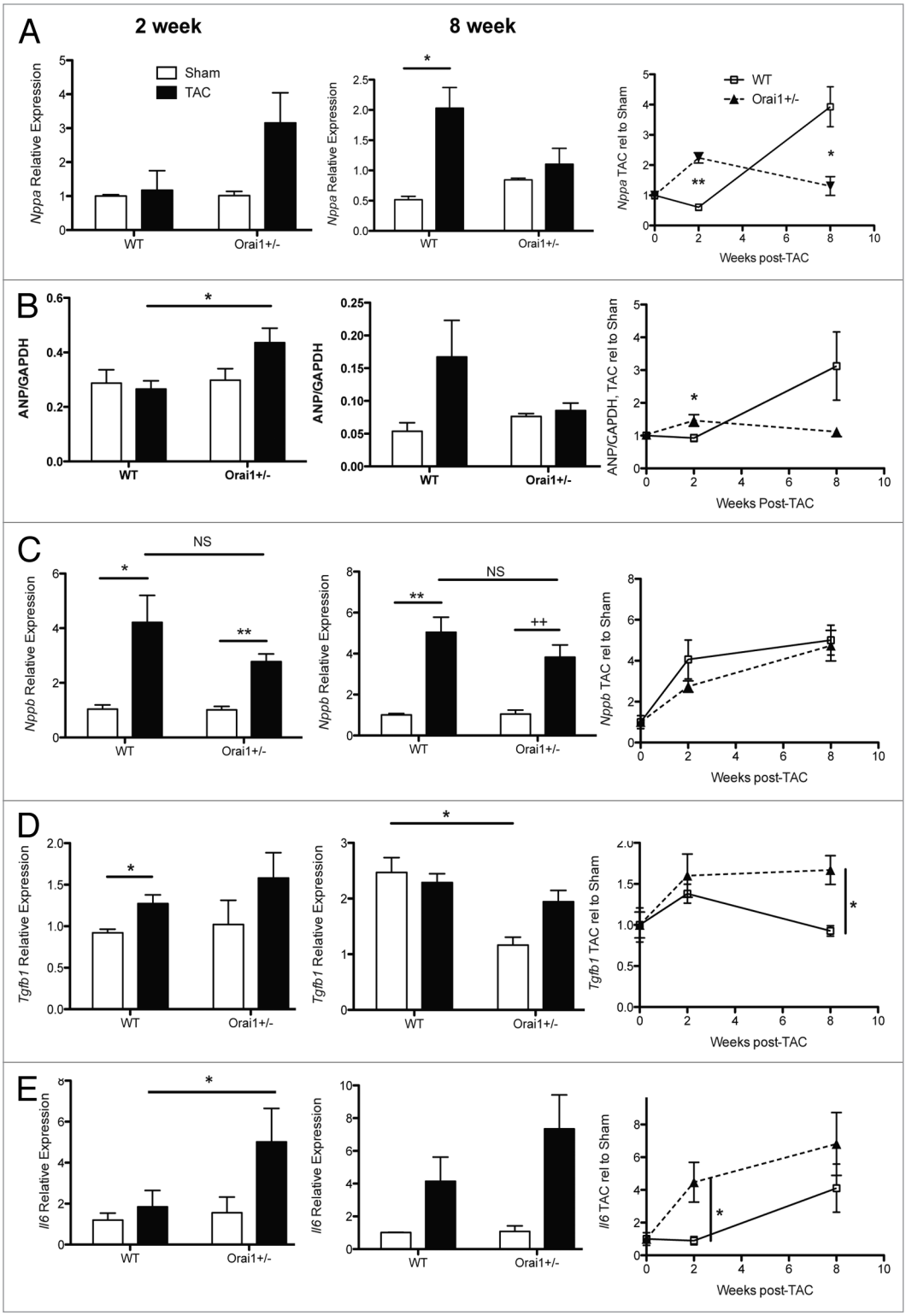

Figure 5. Expression of hypertrophic markers from TAC and sham treated *Orai1*$^{+/-}$ and WT isolated mouse heart lysates. Measurement of mRNA transcripts and protein from heart tissue isolated from TAC and sham treated *Orai1*$^{+/-}$ and WT mice, 2 weeks (left panels), 8 weeks (middle panels) and shown as TAC relative to Sham over time (right panels). (**A**) Transcriptional expression of atrial natriuretic peptide (*Nppa*, ANP) (*p = 0.0422, **p = 0.0012, *p = 0.0246), (**B**) western blot densitometry analysis of *Nppa*, ANP (*p = 0.0303, *p = 0.0393) (**C**) Transcriptional expression analysis of natriuretic peptide (*Nppb*, BNP) (*p = 0.0191, **p = 0.0038, **p = 0.0029, $^{++}$p = 0.007). (**D**) Transcriptional expression analysis of transforming growth factor beta1 (*TGF-β1*) (*p = 0.0187, *p = 0.0496, *p = 0.0163) (**E**) Transcriptional expression analysis of Interleukin-6 (*Il6*) (*p = 0.05, *p = 0.0452).

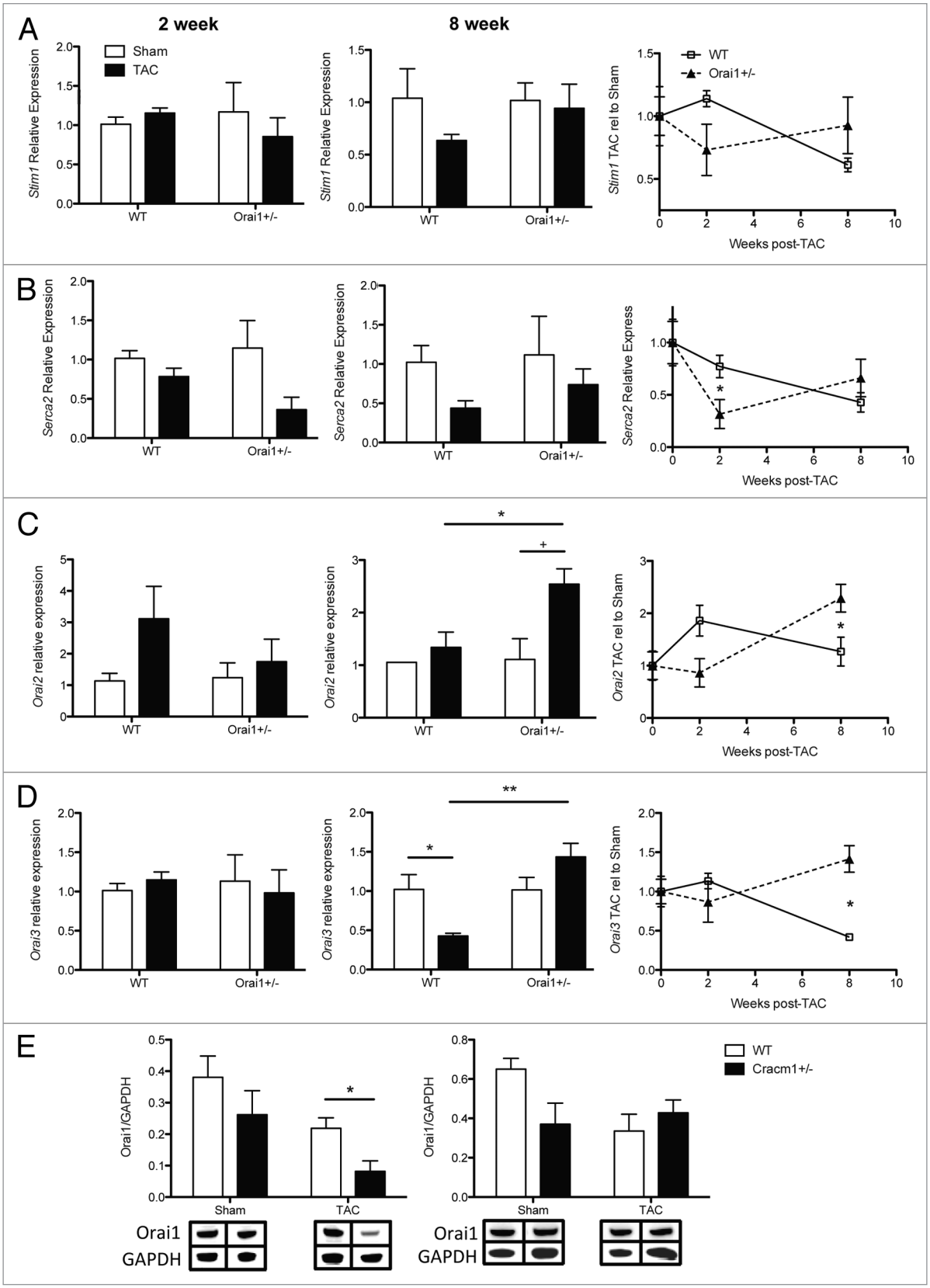

Figure 6. For figure legend, see page 43.

Figure 6 (See previous page). Expression of calcium regulating proteins from TAC and sham treated Orai1$^{+/-}$ and WT isolated mouse heart lysates. Analysis of transcripts and protein from heart tissue isolated from TAC and sham treated *Orai1*$^{+/-}$ and WT mice, 2 weeks (left panels), 8 weeks (middle panels) and shown as TAC relative to Sham over time (right panels). (**A**) Transcriptional expression of Stromal interaction molecule 1 (*Stim1*). (**B**) Transcriptional expression analysis of Sarcoplasmic reticulum Ca^{2+} ATPase (*SERCA2, ATP2A2*) (*p = 0.0449). (**C**) Transcriptional expression analysis of calcium release-activated calcium modulator 2 (*Orai2*) (*p = 0.0437, $^{+}$p = 0.0583 NS, *p = 0.0558). (**D**) Transcriptional expression of *ORAI3* calcium release-activated calcium modulator 3 (Orai3) (*p = 0.0270, **p = 0.0045, *p = 0.0045). (**E**) western blot densitometry analysis of Orai1 protein from heart tissue isolated from TAC and sham treated *Orai1*$^{+/-}$ and WT mice, 2 weeks post TAC (*p = 0.0367), and 8 weeks post TAC. (Bottom panels) representative western blots with bands corresponding to Orai1 and loading control GAPDH.

formed between the ER and the plasma membrane where direct interaction with Orai channels in the plasma membrane controls activation and calcium influx through Orai.[31,32] Transcriptional analysis shows no significant changes in *Stim1* transcript in isolated heart lysates from Sham or TAC-treated WT and *Orai1*$^{+/-}$ mice (**Fig. 6A**).

A key feature of the failing heart is a decrease in SERCA2, which transports Ca^{2+} inside the SR lumen during relaxation of the cardiac myocytes. Transcriptional analysis of *Serca2* shows a similar pattern of transcriptional change to that of other markers analyzed, essentially earlier onset of pathology. In the TAC *Orai1*$^{+/-}$ mice there is significantly less *Serca2* at 2 weeks than in TAC WT mice, compared with their sham controls, returning to similar levels at 8 weeks (**Fig. 6B**).

Transcriptional analysis of *Orai2* and *Orai3* indicate no significant differences between WT and *Orai1*$^{+/-}$ mice at 2 weeks (although expression of *Orai2* may appear to be greater in WT mice), however, both are significantly upregulated at 8 weeks post-TAC in the *Orai1*$^{+/-}$ mice (**Fig. 6C** and **D**). This may indicate a transcriptional program controlled by Orai1. While other markers are changing significantly at 2 weeks, *Orai2* and *3* do not increase in Orai1 deficient mice, yet they increase in WT. They are significantly upregulated at 8 weeks in Orai1 deficient mice, which may indicate some compensatory regulation by the Orai homologs. In *Orai1*$^{+/-}$ mice, we observe less Orai1 protein than in WT mice (**Fig. 6E**).

Apoptosis

Although hypertrophy may serve as an adaptation to increased load on the heart, the growth signals responsible for hypertrophic growth eventually lead to apoptosis. Cardiomyocytes are non-dividing, terminally differentiated cells, so any apoptosis leads to decreased numbers of cardiomyocytes, dilation of the left ventricle and a loss of function in the heart. Given the immediate and significant loss of function in the TAC-treated *Orai1*$^{+/-}$ mice at 2 weeks post-TAC (**Fig. 2**), it is clear that a major lack of compensation to overload is occurring, which could be a result of apoptosis. Analysis of apoptotic markers over this period indicate a significant increase in the amount of apoptosis in TAC-treated *Orai1*$^{+/-}$ mice compared with WT. This is shown by a significant increase of cleaved Caspase 3 protein, as well as the anti-apoptotic Bcl-2 protein, in isolated heart lysates from TAC-treated *Orai1*$^{+/-}$ compared with WT mice at 2 weeks post-TAC (**Fig. 7A** and **C**, **E** and **G**). At 8 weeks post-TAC, WT mice also have a significant increase in cleaved Caspase 3 protein (**Fig. 7B** and **D**). This early onset of apoptosis, and anti-apoptosis signaling, could account for the loss of function during this period, and the earlier development of dilated cardiomyopathy.

Activation of the ERK pathway is linked with cell stretch,[33] and the Ras-Raf-MEK1-ERK1/2 pathway is generally regarded as a pro-hypertrophic and pro-survival pathway that can be a significant but not a necessary signaling component in cardiomyocyte hypertrophy. There is a small but significant increase in phosphorylated vs. total Extracellular signal-regulated kinase, (ERK1/2, MAPK) phosphorylation status, in TAC/Sham treated *Orai1*$^{+/-}$ compared with TAC/Sham treated WT mice at 2 weeks post-TAC, but not later at 8 weeks (**Fig. 8A–D**).

The sarcolemmal recruitment of the AKT/PKB and phosphoinositide-dependent kinase-1 (PDK1) is initiated by the activation of PI3K.[34] When AKT/PKB is activated, compensated cardiac hypertrophy may be induced, although overexpression of AKT/PKB can cause indications and symptoms of cardiac dysfunction.[35] Generally, signaling of AKT/PKB appears to be beneficial to the heart, when activated acutely under physiological conditions.[36] Here we observe a significant increase in phospho-AKT (Ser 473, Protein Kinase B, PKB) relative to total AKT in *Orai1*$^{+/-}$ mice compared with WT mice at 2 and 8 weeks post-TAC (**Fig. 8E–H**).

Discussion

In the present study, we applied a pressure overload model to mice deficient in the store operated calcium channel Orai1 (Cracm1) and compared their response to wild type mice. The Orai1 deficient mice show a significantly reduced survival rate (**Fig. 1A**), a much earlier loss of cardiac function, and an earlier and greater dilation of the left ventricle (**Fig. 2**). This appears to be an acceleration or exacerbation of the disease model, rapidly leading to dilated cardiomyopathy, heart failure and earlier death (**Fig. 1A**).

The significantly increased rate in the loss of function returns to a rate that is similar to that of wild-type pathology later in the disease (**Fig. 2B, D,** and **F**). There is, however, no change in the heart weight early on (**Fig. 1C**) or rate of increase in heart weight (**Fig. 1E**), and no change in cellular hypertrophy (**Fig. 3**), which appears to develop at the same rate. This may suggest that a maximum rate of hypertrophy has been achieved in both wild-type controls and Orai1 deficient mice, but that the Orai1 deficient mice are unable to compensate to the overload, i.e., to yield equivalent functional compensation to wild-type mice.

Concurrent with the loss of function, immediate left ventricle dilation and lack of compensation, we observe a significant increase in anti-apoptosis (Bcl-2), and apoptosis (cleaved Caspase-3) markers (**Fig. 7**).

Our data, and published literature[17,37], suggest that store-operated calcium influx through Orai1 is necessary in order for

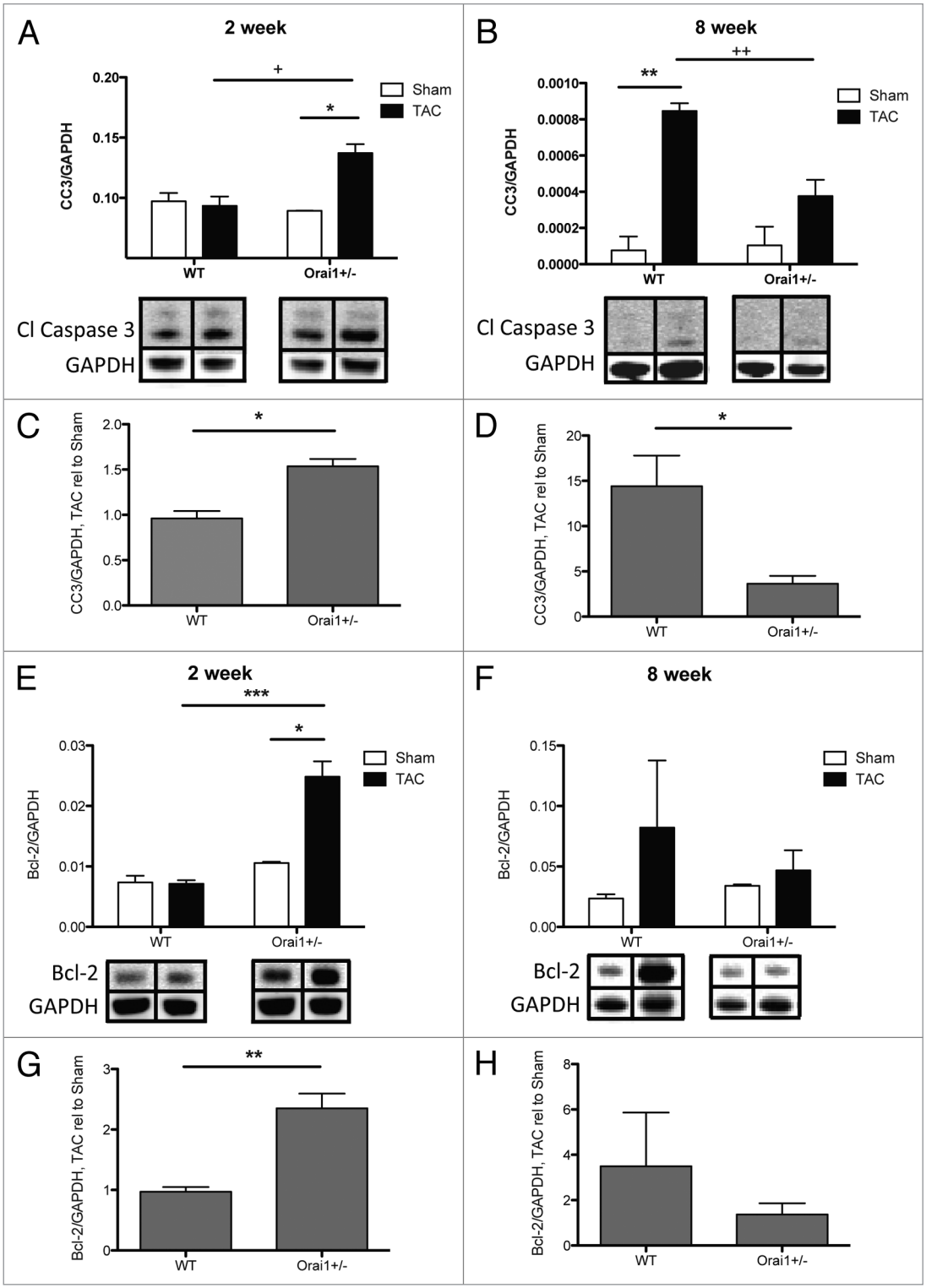

Figure 7. Analysis of apoptotic markers in isolated heart tissue lysates derived from TAC and sham treated Orai1$^{+/-}$ and WT mice. Western blot densitometry analysis of cleaved Caspase 3 (CASP3) protein from heart tissue isolated from TAC and sham treated *Orai1*$^{+/-}$ and WT mice, (**A**) 2 weeks post TAC (*p = 0.0228; $^{+}$p = 0.0254), and (**B**) 8 weeks post TAC (**p = 0.0023; $^{++}$p = 0.0092). (Bottom panels) representative western blots with bands corresponding to cleaved Caspase 3 and loading control GAPDH. Analysis of cleaved Caspase 3 western blot densitometry, showing TAC relative to Sham at (**C**) 2 weeks post TAC (*p = 0.0119), and (**D**) 8 weeks post TAC (*p = 0.0456). Western blot densitometry analysis of Bcl-2 (B-cell lymphoma 2) protein from heart tissue isolated from TAC and sham treated *Orai1*$^{+/-}$ and WT mice, (**E**) 2 weeks post TAC (*p = 0.0230, ***p = 0.0005), and (**F**) 8 weeks post TAC. (Bottom panels) Representative western blots with bands corresponding to Bcl-2 and loading control GAPDH. Analysis of Bcl-2 western blot densitometry, showing TAC relative to Sham at (**G**) 2 weeks post TAC (**p = 0.0016), and (**H**) 8 weeks post TAC.

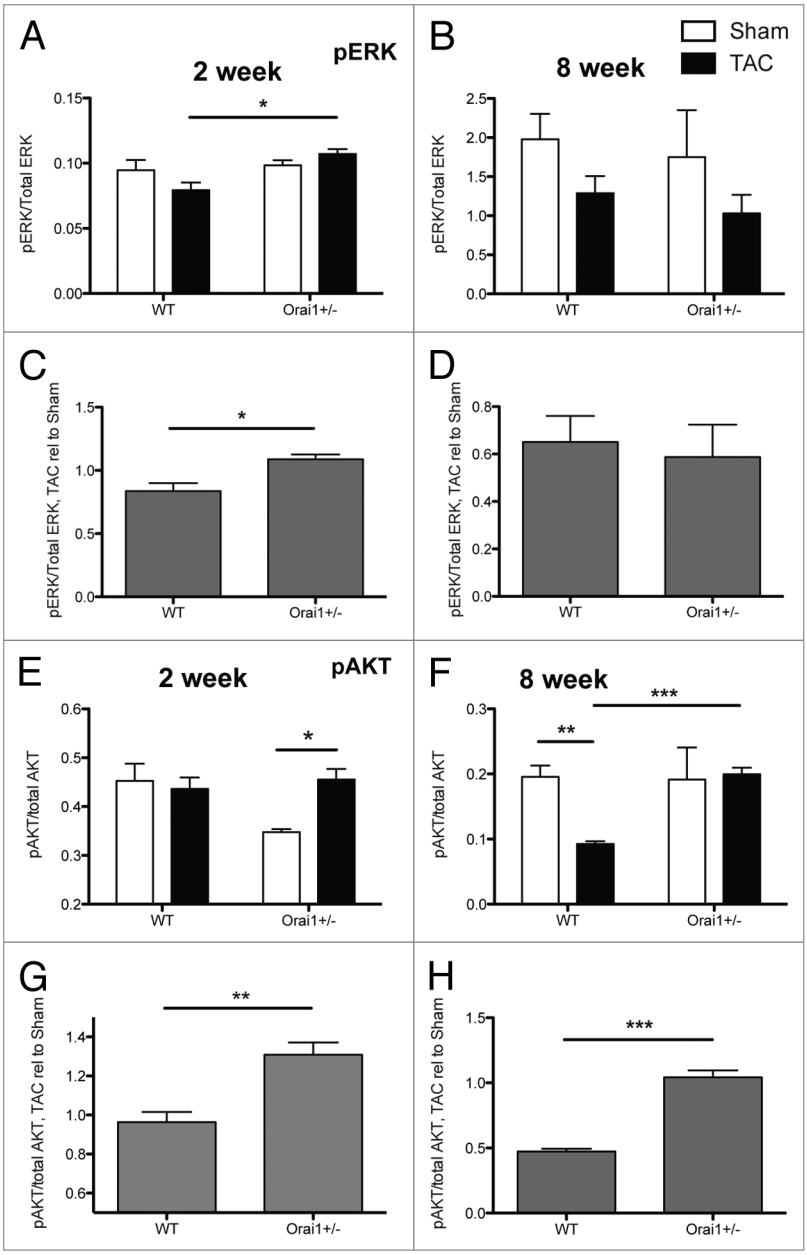

Figure 8. Analysis of phosphorylated protein markers in isolated heart tissue lysates derived from TAC and sham treated Orai1$^{+/-}$ and WT mice. Western blot densitometry analysis of Extracellular signal-regulated kinase, (ERK1/2, MAPK) phosphorylation status; shown as phosphorylated ERK (Thr202/Tyr204) relative to total ERK at (**A**) 2 weeks post TAC (*p = 0.0154), and (**B**) 8 weeks post TAC. Analysis of phospho-ERK/total-ERK western blot densitometry, showing TAC relative to Sham at (**C**) 2 weeks post TAC (*p = 0.0266), and (**D**) 8 weeks post TAC. Western blot densitometry analysis of AKT (Protein Kinase B, PKB) phosphorylation status; phosphorylated AKT (Ser473), relative to total AKT at (**E**) 2 weeks post TAC (*p = 0.0325), and (**F**) 8 weeks post TAC (**p = 0.0052, ***p = 0.0006). Analysis of phospho-AKT/total-AKT. Western blot densitometry, showing TAC relative to Sham at (**G**) 2 weeks post TAC (**p = 0.0078), and (**H**) 8 weeks post TAC (***p = 0.0005).

myocytes to respond to changing demands. Without calcium influx through Orai1, cardiomyocytes may be unable to respond to additional load, greatly upregulating stretch response, hypertrophic markers, and anti-apoptotic proteins (Bcl-2). Unable to compensate and prevent the apoptotic cascade, cardiomyocytes start to fail and die, and the tissue remodels, becoming fibrotic and rigid, exacerbating the overload, leading to further loss of function, dilated cardiomyopathy, and eventually heart failure. The response to deficient Orai1-mediated calcium influx most likely combines a defective calcium-mediated transcriptional response program with an acute deficiency in the additional calcium necessary to immediately enhance cardiomyocyte contraction, to compensate for additional load.

Orai1, and its associated current I_{CRAC}, are fundamental control points in the immediate activation of cells of the immune system and in the elicitation of various immune responses.[6-13] Compounding pathology, especially interstitial tissue remodeling, infiltration and inflammatory programs could also result from a dysregulation of immunocyte activation via Orai1 deficiency.

It is clear that Orai1 plays a critical role in the progression of heart failure and dilated cardiomyopathy, and could potentially provide a therapeutic target for small molecule regulators.

Methods

Animal care

All animal procedures were approved by the Institutional Animal Care and Use Committee at the University of Hawaii.

Animals

Initial mice were a gift from Drs Vig and Kinet.[38] These Orai1 deficient mice were generated using Genetrap,[39] with the gene-trapping cassette inserted in the 1st intron in the ES cells.[38] These mice were crossed with C57BL/6J for nine generations. Homozygous deletion of *Orai1* in a C57BL/6 background results in embryonic and perinatal lethality.[31,40,41] Mice with heterozygous deletion of *Orai1* developed normally, leading to viable mice with approximately two thirds to a half of the protein levels of the corresponding ORAI1, with no significant changes in basal levels of the other Orai homologs (**Fig. 6**). C57BL/6J were used as WT control animals. Mice were housed under a 12-h light/dark cycle and fed with standard diet and water ad libitum. Ten-week-old male mice were used for all experiments. Two and eight weeks after surgery, mice were euthanized by CO_2 asphyxiation for histological and molecular analyses.

Transverse Aortic Constriction (TAC)

Transverse aortic constriction was performed, producing left ventricular hypertrophy by constriction of the aorta.[22,42-44] Briefly, the left side of the chest was depilated with Nair and a baseline 2-D echocardiogram was obtained as described below. Mice were then deeply anesthetized with a

mixture of ketamine and xylazine. The transverse aorta between the brachiocephalic and left carotid artery was banded using 6–0 silk ligature around the vessel and a 26G blunt needle, after which the needle was withdrawn. Sham surgeries were identical apart from the constriction of the aorta.

Doppler echocardiography

Doppler echocardiography was performed one week post-TAC to measure the level of constriction. Mice were anesthetized lightly with isofluorene gas and shaved. Doppler echocardiography was performed using the Visualsonics Vevo 770 system (http://www.visualsonics.com/vevo770). In the parasternal short-axis view, the pulsed wave Doppler sample volume was placed in the transverse aorta just proximal and distal to the site of banding. Peak velocity was traced using Vevo 770 software, and the pressure gradient was calculated using the simplified Bernoulli equation.

Transthoracic echocardiography

Baseline and post-TAC transthoracic echocardiography were used to assess changes in mouse heart dimensions and function. Briefly, after two days of acclimatization and depilation, unanesthetized transthoracic echocardiography was performed at 2, 4, 6, and 8 wks post-TAC or Sham, using a 30-Mhz transducer (Vevo 770, VisualSonics). High quality 2-D images and M-mode images of the left ventricle were recorded. Measurements of left ventricular end-diastolic (LVIDd) and end-systolic (LVIDs) internal dimensions were performed by the leading edge to leading edge convention adopted by the American Society of Echocardiography. The left ventricular ejection fraction (%EF) was calculated as (LV Vol; d-LV Vol;s/LV Vol; d x 100), The left ventricular fractional shortening (%FS) was calculated as [(LVID,d – LVID,s) / LVID,d] x 100%. (Visualsonics Inc.).

Tissue preparation for histology

Two or 8 weeks post-TAC or sham, mice were euthanized by CO_2 asphyxiation and hearts were collected for histological and molecular analysis. For histology, hearts were perfused with phosphate-buffered saline and 10% formalin or zinc fixative (BD) in situ, collected immediately, and fixed overnight in 10% formalin at 4°C or zinc fixative at room temperature. Tissues were then cut in a sagittal orientation, embedded in paraffin, mounted on glass slides, and stored until use. Paraffin-embedded sections were stained for the following:

Collagen

Collagen volume fraction was determined by analysis of picrosirius stained sections. Sections cut to 5-μm thickness were deparaffinized, rehydrated and stained with picrosirius red (0.1% Sirius Red in picric acid). Sections were subsequently washed and dehydrated before image analysis.

Cardiomyocyte cross sectional area

Heart sections were deparaffinized and permeabilized, then stained with wheat germ agglutinin conjugated to Alexa Fluor 488 (WGA-Alexa Fluor 488, Invitrogen, W11261) (http://www.lifetechnologies.com/order/catalog/product/W11261) at a concentration of 50 μg/mL to identify sarcolemmal membranes and measure cardiomyocyte cross sectional area (described below). Nuclei were visualized with Hoechst 3649.

Image collection and analysis

Fluorescent and bright field images were collected on an epifluorescence microscope (Axioscope, Zeiss). Fibrosis and cross-sectional cardiomyocyte area were quantified using ImageJ software (NIH). To quantify fibrosis, collagen fibers were highlighted, and the red-stained pixels were counted to determine the percentage of pixels in each field that represented collagen fibers. Perivascular tissue was excluded from this calculation. One section (2 halves of a heart) from each animal was imaged at 10 images per heart, with a minimum of 3 animals per experimental group. Data values were averaged for each animal and graphed in Prism (GraphPad). Cardiomyocytes from WGA stained sections were randomly selected in a blinded fashion then traced to determine the cross sectional area of individual myocytes (n = 100). All images were captured and analyzed in a single-blind manner.

Real-time PCR

For RNA extraction, hearts were collected from mice and total RNA was isolated from homogenized hearts with Trizol (Molecular Research Center, TR 118) (http://mrc.ws/catalog/product_info.php?cPath=1&products_id=38) and further purified with an RNA isolation kit (Mo Bio Laboratories, Inc., 15000–250) (http://www.mobio.com/tissue-cells-rna-isolation/). Single-stranded cDNA was synthesized from 300ng of RNA using the qScript cDNA Super Mix (Quanta Biosciences) (http://www.quantabio.com/product.php?base_id=95048). The mRNA levels of atrial natriuretic peptide Nppa, Tgfb1, Col3a1, matrix metalloproteinase (MMP) 2 and 9, cyclophilin (ppia) were quantified by real-time PCR in triplicate with QuantiTect SYBR Green (Life Technologies) (http://www.lifetechnologies.com/us/en/home/life-science/pcr/real-time-pcr/real-time-pcr-reagents/sybr-green-real-time-master-mixes.html) on an ABI 7900HT Fast Real-Time PCR System (Life Technologies) using the following cycling conditions: 2 min at 50°C, 10 min at 95°C, followed by 40 cycles of 15 s at 95°C, 1 min at 60°C. The following primer pairs were used: *Nppa*: 5′AGA AAC CAG AGA GTG GGC AGA G 3′; 5′ CAA GAC GAG GAA GAA GCC CAG 3′; *Nppb*: 5′ GCG GCA TGG ATC TCC TGA AGG 3′; 5′ CCC AGG CAG AGT CAG AAA CTG 3′; *Tgfb1*: 5′ TGG AGC AAC ATG TGG AAC TC 3′; 5′ CAG CAG CCG GTT ACC AAG 3′; *Col3a1*: 5′ GAC CGA TGG ATT CCA GTT CG 3′; 5′ TGT GAC TCG TGC AGC CAT CC 3′; *Il6*: 5′ AGA AGG AGT GGC TAA GGA CCA A 3′; 5′ GCA TAA CGC ACT AGG TTT GCC 3′; *Stim1*: 5′ CTG GAC TGT GGA TGA GGT GAT A 3′; 5′ TGG TGG TGT TGG TTA CTG CTA 3′; *Serca2*: 5′ AAC CTT GCT GGA ACT TGT GAT T 3′; 5′ CAG TAT GCT TGA TGA CGG AGA C 3′; *Orai2*: 5′ GGC ATG GAT TAC CGA GAC TG 3′; 5′ GGT GAA GAC CAC GAA GAT GAG 3′; *Orai3*: 5′ CGG CTA CCT GGA CCT TAT GG 3′; 5′ TTG CTC ACG GCT TCA ATA TGG 3′; *Ppia* (cyclophilin A): 5′ CAA AGT TCC AAA GAC AGC AGA AAA C 3′; 5′ GGC ACA TGA ATC CTG GAA TAA TTC 3′. Relative quantitation was performed using the comparative (ΔΔCt) method (ABI User Bulletin #2).

Western blot analysis

Hearts were collected and protein extracts were prepared from homogenized heart tissue in lysis buffer (75 mM NaCl, 40 min mM NaF, 10 mM Iodoacetamide, 50 mM HEPES, 10% IGEPAL, 0.5 mM PMSF) containing protease inhibitors (Complete Protease Inhibitor Cocktail, Roche) (http://www.roche.com/products/product-details.htm?type=product&id=104). Total protein concentrations were determined by the bicinchoninic acid (BCA) colorimetric assay. Absorbance was measured at 562 nm by spectrophotometer (Spectra Max 340) and concentrations determined using a standard curve based on bovine serum albumin (BSA) protein standards. Concentrations were normalized to 30 μg and separated on a 4–12% Polyacrylamide Bis-Tris gel (Life Technologies) (http://www.lifetechnologies.com/order/catalog/product/NP0323BOX). Protein samples were transferred to polyvinylidene fluoride (PVDF) membrane and blocked with Odyssey Blocking Buffer (Li-Cor) (http://www.licor.com/bio/products/reagents/odyssey_blocking_buffer/odyssey_blocking_buffer.jsp). Membranes were probed overnight at 4°C with antibodies to full-length ANP, MMP2, Bcl-2 (Santa Cruz), cleaved caspase-3, phospho- and total p44/42 MAPK (Erk1/2), and GAPDH (Calbiochem). Protein was visualized utilizing secondary antibodies designed for a Li-Cor Oddysey infrared scanner with the reagents and recommended protocol of the manufacturer, and quantitated with Image Studio software (Li-Cor).

Statistics

Statistical significance of echocardiography data was evaluated using 2-way ANOVA, with a Bonferroni post hoc test and linear regression. Histology and molecular data were evaluated using the 2-tailed Student t-test. Evaluations were performed using PRISM software with $p < 0.05$ regarded as significant. All data are shown as mean +/− SEM.

Disclosure of Potential Conflicts of Interest

No potential conflicts of interest were disclosed.

Acknowledgments

The authors would like to acknowledge Drs Monica Vig and Jean-Pierre Kinet for their gift of the Orai1 knockout mice.

Sources of funding

This work was supported by grants from: National Institutes of Health, NIMHD-BRIC P20 MD006084, NIMHD-RCMI-BRIDGES G12 MD007601, and the Hawaii Community Foundation, Leahi Fund 13ADVC-60228. Support for the imaging and histology core facilities was provided by a Research Centers in Minority Institutions grant from the National Institute on Minority Health and Health Disparities (G12 MD007601). Support for the INBRE in vivo core was provided by a grant from the National Institute of General Medicine NIGMS-INBRE P20 GM103466.

References

1. Hou X, Pedi L, Diver MM, Long SB. Crystal structure of the calcium release-activated calcium channel Orai. Science 2012; 338:1308-13; PMID:23180775; http://dx.doi.org/10.1126/science.1228757
2. Prakriya M, Feske S, Gwack Y, Srikanth S, Rao A, Hogan PG. Orai1 is an essential pore subunit of the CRAC channel. Nature 2006; 443:230-3; PMID:16921383; http://dx.doi.org/10.1038/nature05122
3. Putney JW Jr. A model for receptor-regulated calcium entry. Cell Calcium 1986; 7:1-12; PMID:2420465; http://dx.doi.org/10.1016/0143-4160(86)90026-6
4. González-Cobos JC, Zhang X, Zhang W, Ruhle B, Motiani RK, Schindl R, Muik M, Spinelli AM, Bisaillon JM, Shinde AV, et al. Store-independent Orai1/3 channels activated by intracrine leukotriene C4: role in neointimal hyperplasia. Circ Res 2013; 112:1013-25; PMID:23349245; http://dx.doi.org/10.1161/CIRCRESAHA.111.300220
5. Soboloff J, Madesh M, Gill DL. Sensing cellular stress through STIM proteins. Nat Chem Biol 2011; 7:488-92; PMID:21769090; http://dx.doi.org/10.1038/nchembio.619
6. Lewis RS. Calcium signaling mechanisms in T lymphocytes. Annu Rev Immunol 2001; 19:497-521; PMID:11244045; http://dx.doi.org/10.1146/annurev.immunol.19.1.497
7. Lewis RS. The molecular choreography of a store-operated calcium channel. Nature 2007; 446:284-7; PMID:17361175; http://dx.doi.org/10.1038/nature05637
8. Hoth M, Penner R. Calcium release-activated calcium current in rat mast cells. J Physiol 1993; 465:359-86; PMID:8229840
9. Hoth M, Penner R. Depletion of intracellular calcium stores activates a calcium current in mast cells. Nature 1992; 355:353-6; PMID:1309940; http://dx.doi.org/10.1038/355353a0
10. Hogan PG, Rao A. Dissecting ICRAC, a store-operated calcium current. Trends Biochem Sci 2007; 32:235-45; PMID:17434311; http://dx.doi.org/10.1016/j.tibs.2007.03.009
11. Hogan PG, Chen L, Nardone J, Rao A. Transcriptional regulation by calcium, calcineurin, and NFAT. Genes Dev 2003; 17:2205-32; PMID:12975316; http://dx.doi.org/10.1101/gad.1102703
12. Oh-hora M, Rao A. Calcium signaling in lymphocytes. Curr Opin Immunol 2008; 20:250-8; PMID:18515054; http://dx.doi.org/10.1016/j.coi.2008.04.004
13. Feske S. Calcium signalling in lymphocyte activation and disease. Nat Rev Immunol 2007; 7:690-702; PMID:17703229; http://dx.doi.org/10.1038/nri2152
14. Hara M, Ono K, Hwang MW, Iwasaki A, Okada M, Nakatani K, Sasayama S, Matsumori A. Evidence for a role of mast cells in the evolution to congestive heart failure. J Exp Med 2002; 195:375-81; PMID:11828013; http://dx.doi.org/10.1084/jem.20002036
15. Dombrowicz D, Flamand V, Miyajima I, Ravetch JV, Galli SJ, Kinet JP. Absence of Fc epsilonRI alpha chain results in upregulation of Fc gammaRIII-dependent mast cell degranulation and anaphylaxis. Evidence of competition between Fc epsilonRI and Fc gammaRIII for limiting amounts of FcR beta and gamma chains. J Clin Invest 1997; 99:915-25; PMID:9062349; http://dx.doi.org/10.1172/JCI119256
16. Cimini M, Fazel S, Zhuo S, Xaymardan M, Fujii H, Weisel RD, Li RK. c-kit dysfunction impairs myocardial healing after infarction. Circulation 2007; 116(Suppl):I77-82; PMID:17846329; http://dx.doi.org/10.1161/CIRCULATIONAHA.107.708107
17. Stiber JA, Rosenberg PB. The role of store-operated calcium influx in skeletal muscle signaling. Cell Calcium 2010; PMID:21176846
18. Kawasaki T, Ueyama T, Lange I, Feske S, Saito N. Protein kinase C-induced phosphorylation of Orai1 regulates the intracellular Ca2+ level via the store-operated Ca2+ channel. J Biol Chem 2010; 285:25720-30; PMID:20534587; http://dx.doi.org/10.1074/jbc.M109.022996
19. McCarl CA, Picard C, Khalil S, Kawasaki T, Röther J, Papolos A, Kutok J, Hivroz C, Ledeist F, Plogmann K, et al. ORAI1 deficiency and lack of store-operated Ca2+ entry cause immunodeficiency, myopathy, and ectodermal dysplasia. J Allergy Clin Immunol 2009; 124:1311-8, e7; PMID:20004786; http://dx.doi.org/10.1016/j.jaci.2009.10.007
20. Voelkers M, Salz M, Herzog N, Frank D, Dolatabadi N, Frey N, Gude N, Friedrich O, Koch WJ, Katus HA, et al. Orai1 and Stim1 regulate normal and hypertrophic growth in cardiomyocytes. J Mol Cell Cardiol 2010; 48:1329-34; PMID:20138887; http://dx.doi.org/10.1016/j.yjmcc.2010.01.020
21. Patten RD, Hall-Porter MR. Small animal models of heart failure: development of novel therapies, past and present. Circ Heart Fail 2009; 2:138-44; PMID:19808329; http://dx.doi.org/10.1161/CIRCHEARTFAILURE.108.839761
22. Rockman HA, Ono S, Ross RS, Jones LR, Karimi M, Bhargava V, Ross J Jr., Chien KR. Molecular and physiological alterations in murine ventricular dysfunction. Proc Natl Acad Sci U S A 1994; 91:2694-8; PMID:8146176; http://dx.doi.org/10.1073/pnas.91.7.2694
23. Lygate C. Surgical models of hypertrophy and heart failure: Myocardial infarction and transverse aortic constriction. Drug Discov Today Dis Models 2006; 3:283-90; http://dx.doi.org/10.1016/j.ddmod.2006.10.002
24. Berk BC, Fujiwara K, Lehoux S. ECM remodeling in hypertensive heart disease. J Clin Invest 2007; 117:568-75; PMID:17332884; http://dx.doi.org/10.1172/JCI31044

25. Creemers EE, Pinto YM. Molecular mechanisms that control interstitial fibrosis in the pressure-overloaded heart. Cardiovasc Res 2011; 89:265-72; PMID:20880837; http://dx.doi.org/10.1093/cvr/cvq308
26. Bergman MR, Teerlink JR, Mahimkar R, Li L, Zhu BQ, Nguyen A, Dahi S, Karliner JS, Lovett DH. Cardiac matrix metalloproteinase-2 expression independently induces marked ventricular remodeling and systolic dysfunction. Am J Physiol Heart Circ Physiol 2007; 292:H1847-60; PMID:17158653; http://dx.doi.org/10.1152/ajpheart.00434.2006
27. Dobaczewski M, Chen W, Frangogiannis NG. Transforming growth factor (TGF)-β signaling in cardiac remodeling. J Mol Cell Cardiol 2011; 51:600-6; PMID:21059352; http://dx.doi.org/10.1016/j.yjmcc.2010.10.033
28. Barry SP, Davidson SM, Townsend PA. Molecular regulation of cardiac hypertrophy. Int J Biochem Cell Biol 2008; 40:2023-39; PMID:18407781; http://dx.doi.org/10.1016/j.biocel.2008.02.020
29. Thum T, Galuppo P, Wolf C, Fiedler J, Kneitz S, van Laake LW, Doevendans PA, Mummery CL, Borlak J, Haverich A, et al. MicroRNAs in the human heart: a clue to fetal gene reprogramming in heart failure. Circulation 2007; 116:258-67; PMID:17606841; http://dx.doi.org/10.1161/CIRCULATIONAHA.107.687947
30. Lai NC, Gao MH, Tang E, Tang R, Guo T, Dalton ND, Deng A, Tang T. Pressure overload-induced cardiac remodeling and dysfunction in the absence of interleukin 6 in mice. Lab Invest 2012; 92:1518-26; PMID:22825686; http://dx.doi.org/10.1038/labinvest.2012.97
31. Cahalan MD. STIMulating store-operated Ca(2+) entry. Nat Cell Biol 2009; 11:669-77; PMID:19488056; http://dx.doi.org/10.1038/ncb0609-669
32. Soboloff J, Rothberg BS, Madesh M, Gill DL. STIM proteins: dynamic calcium signal transducers. Nat Rev Mol Cell Biol 2012; 13:549-65; PMID:22914293; http://dx.doi.org/10.1038/nrm3414
33. Yazaki Y, Komuro I. Role of protein kinase system in the signal transduction of stretch-mediated myocyte growth. Basic Res Cardiol 1992; 87(Suppl 2):11-8; PMID:1338562
34. Cantley LC. The phosphoinositide 3-kinase pathway. Science 2002; 296:1655-7; PMID:12040186; http://dx.doi.org/10.1126/science.296.5573.1655
35. Condorelli G, Drusco A, Stassi G, Bellacosa A, Roncarati R, Iaccarino G, Russo MA, Gu Y, Dalton N, Chung C, et al. Akt induces enhanced myocardial contractility and cell size in vivo in transgenic mice. Proc Natl Acad Sci U S A 2002; 99:12333-8; PMID:12237475; http://dx.doi.org/10.1073/pnas.172376399
36. Heineke J, Molkentin JD. Regulation of cardiac hypertrophy by intracellular signalling pathways. Nat Rev Mol Cell Biol 2006; 7:589-600; PMID:16936699; http://dx.doi.org/10.1038/nrm1983
37. Olivetti G, Abbi R, Quaini F, Kajstura J, Cheng W, Nitahara JA, Quaini E, Di Loreto C, Beltrami CA, Krajewski S, et al. Apoptosis in the failing human heart. N Engl J Med 1997; 336:1131-41; PMID:9099657; http://dx.doi.org/10.1056/NEJM199704173361603
38. Vig M, DeHaven WI, Bird GS, Billingsley JM, Wang H, Rao PE, Hutchings AB, Jouvin MH, Putney JW, Kinet JP. Defective mast cell effector functions in mice lacking the CRACM1 pore subunit of store-operated calcium release-activated calcium channels. Nat Immunol 2008; 9:89-96; PMID:18059270; http://dx.doi.org/10.1038/ni1550
39. Skarnes WC. Gene trapping methods for the identification and functional analysis of cell surface proteins in mice. Methods Enzymol 2000; 328:592-615; PMID:11075368; http://dx.doi.org/10.1016/S0076-6879(00)28420-6
40. McCarl CA, Khalil S, Ma J, Oh-hora M, Yamashita M, Roether J, Kawasaki T, Jairaman A, Sasaki Y, Prakriya M, et al. Store-operated Ca2+ entry through ORAI1 is critical for T cell-mediated autoimmunity and allograft rejection. J Immunol 2010; 185:5845-58; PMID:20956344; http://dx.doi.org/10.4049/jimmunol.1001796
41. Bergmeier W, Oh-Hora M, McCarl CA, Roden RC, Bray PF, Feske S. R93W mutation in Orai1 causes impaired calcium influx in platelets. Blood 2009; 113:675-8; PMID:18952890; http://dx.doi.org/10.1182/blood-2008-08-174516
42. Horton JS, Buckley CL, Stokes AJ. Successful TRPV1 antagonist treatment for cardiac hypertrophy and heart failure in mice. Channels (Austin) 2013; 7:17-22; PMID:23221478; http://dx.doi.org/10.4161/chan.23006
43. Buckley CL, Stokes AJ. Corin-deficient W-sh mice poorly tolerate increased cardiac afterload. Regul Pept 2011; 172:44-50; PMID:21903139; http://dx.doi.org/10.1016/j.regpep.2011.08.006
44. Buckley CL, Stokes AJ. Mice lacking functional TRPV1 are protected from pressure overload cardiac hypertrophy. Channels (Austin) 2011; 5:367-74; PMID:21814047; http://dx.doi.org/10.4161/chan.5.4.17083